Out-of-plane beam shaping with UV-written tilted Bragg gratings for beam delivery on quantum chips

DONG-WOO KO*, Q. SALMAN AHMED, JAMES W. FIELD, JAMES C. GATES, PETER HORAK

Optoelectronics Research Centre, University of Southampton, Southampton SO17 1BJ, UK
d-w.ko@soton.ac.uk

Abstract: We theoretically and numerically investigate the performance of tilted Bragg gratings in planar waveguides, fabricated by direct UV writing in photosensitive silica, to couple light out of a chip. An analytic expression is derived for the coupling efficiency and validated numerically by finite element simulations. Using the analytic result, we can design gratings to generate output beams in free space of any specific shape and calculate their overall power coupling efficiency. Our simulations indicate that for currently achievable grating index contrasts devices of millimeter length are most suitable for this technology.

1. Introduction

The development of quantum technology allows us to innovate our conventional devices, boosting their performance in efficiency and sensitivity. Examples of this include gravity sensors [1], magnetic imaging in healthcare [2], secure methods of communication [3], and computing [4–6]. Many of these devices rely on the manipulation of trapped clouds of neutral atoms or trapped ions by laser beams, but so far optical access is mainly achieved by free space optics. Devices such as monolithic ion-traps [7], membrane and needle magneto-optical traps (MOTs) [8, 9], and grating MOTs [10] are beginning to utilize integrated waveguides incorporated directly into the chip design, eliminating the need for bulky free space optics. Such compactness is sought after for quantum applications, especially for highly complex devices such as quantum computers where scalability is extremely challenging [11, 12] and photonic integration can offer a solution.

A common approach to combining integrated waveguides and free space beams is to use etched grating couplers [13–16], which provide efficient coupling over short devices of sub-millimeter lengths. An alternative technology for grating fabrication is direct UV writing [17–21] which avoids any issues of surface roughness and non-uniformity and therefore has the potential to deliver higher quality beams than etched gratings. In this case the grating is formed using an interference pattern from two UV laser beams inside a photo-sensitive waveguide. This process guarantees a smooth and continuous refractive index profile of the fabricated holographic grating but is limited in the achievable refractive index contrast and thus in the light coupling efficiency.

In this paper we investigate theoretically and by numerical simulations the achievable efficiency of direct UV-written Bragg gratings to couple light from integrated silica waveguides 'out-of-plane' and into free space. To achieve this the grating planes need to be tilted with respect to the waveguide's transverse direction, thus adding to the fabrication complexity but providing highly controllable directionality of the out-coupled light. We demonstrate how this directionality can be exploited to shape the light beam out-coupled into any target profile, e.g., to address individual ions or atom clouds at specific positions above the chip surface, and we calculate the overall power coupling efficiency.

This paper is structured as follows. In Sec. 2 we discuss the device geometry used for our analysis and the refractive index profile of the UV-written tilted Bragg gratings. Sec. 3 derives an

analytic solution for the grating coupling efficiency of uniform gratings as a function of grating parameters which is then analyzed and compared with finite element simulations. In Sec. 4 we discuss and demonstrate a method to design gratings that generate out-coupled beams of any given target shape and direction and calculate the power coupling efficiencies of such beam shaping devices. Finally, we conclude in Sec. 5.

2. Device geometry

The basic geometry of the system under investigation is shown in Fig. 1. The device consists of a photosensitive hydrogen-loaded silica core layer which is sandwiched between lower refractive index silica undercladding and overcladding layers. By direct UV writing, an optical waveguide and tilted Bragg gratings are formed in the photosensitive core layer. The grating couples light out of the waveguide into the first diffraction order, through the overcladding layer, and into free space above the sample. Our work aims to design the grating so that the diffracted light beam is shaped and focused on a specific target position above the device.

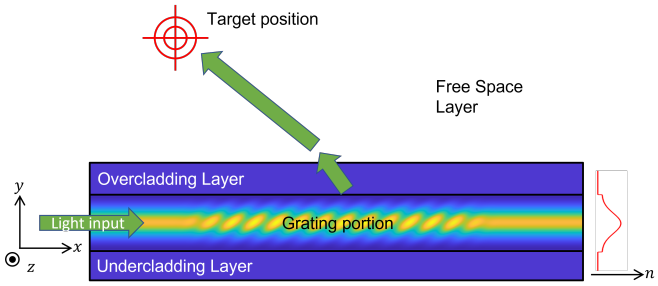

Fig. 1. Schematics of the device geometry: light is propagating through the waveguide core layer, diffracted out by the tilted grating, and focused on the target position above the sample. The waveguide index profile is shown on the right.

For our theoretical and numerical models we consider a simplified two-dimensional geometry, i.e., we assume that the device is infinitely extended in the third, z direction. In practice, our model is thus applicable to three-dimensional waveguides that are wide enough in z so that the beam divergence in this direction can be neglected, i.e., that the distance to the target position is below the transverse, z, Rayleigh length of the beam diffracted out of the grating. The propagation direction of light in the waveguide is given by x, the vertical direction is denoted by y, as shown in Fig. 1.

Each layer of the device has a specific refractive index distribution. Both cladding layers have a constant refractive index and the refractive index of air is set to 1. The core layer with the direct UV-written waveguide and tilted Bragg grating has a refractive index profile of [22]

$$n_g(x,y) = n_{co} + \left[\Delta n + \Delta n_g(x)\sin\left(2\pi\frac{x - y\tan\theta}{\Lambda}\right)\right]\exp\left(-\frac{y^2}{\sigma^2}\right) \tag{1}$$

where n_{co} is the core index, Δn is an additional index induced onto the waveguide by UV-writing, $\Delta n_g(x)$ is the grating index contrast, θ is the tilt angle of the grating planes, Λ is the grating period, and σ is the width of the waveguide and grating, assumed to have a Gaussian transverse shape in the y-axis. The x-dependence of the grating profile $\Delta n_g(x)$ indicates that the grating only occupies a part of the device length ($\Delta n_g(x) = 0$ in regions of the waveguide without the grating) and allows for an apodization of the grating to suppress stray light diffracted from an abrupt change in refractive index.

We combine several methods to simulate light propagation in the device. For the diffraction of light by the tilted grating we develop an analytical method, see Sec. 3.1 below. This is then

compared with simulations using a commercial finite element method (FEM) solver (Comsol Multiphysics®) with a mapped mesh in the 2D rectangular geometry. Propagation in free space and the cladding layers as well as refraction at the glass-air interface is calculated using an angular spectrum method programmed in Matlab, taking the analytical or FEM-calculated diffracted field from the core region as input.

3. Coupling of uniform gratings

3.1. Analytic diffraction theory

First, we derive an analytic expression for the electric field of the light diffracted out of the waveguide by the direct UV-written tilted Bragg grating with a refractive index distribution given by Eq. (1). This is calculated by the beam tracing method [23] and extends previous results [22,23] that only considered a tilt angle of 45° to arbitrary tilt angles θ. We start by assuming that the electric field $f(y)$ of the fundamental mode of the waveguide can by approximated by a Gaussian beam of width w_0,

$$f(y) = \exp(-y^2/w_0^2). \tag{2}$$

Next, the grating is approximated as a large number M per grating period Λ of thin parallel slices of constant refractive index angled at the tilt angle of the grating, where the m-th slice at position $x_m = \Lambda m/M$ has a refractive index on axis of $n_m = n_{co} + \Delta n + \Delta n_g \sin(2\pi m/M)$. The Fresnel coefficient for s-polarization, i.e., polarization in z direction in our coordinate system of Fig. 1, for the reflection of the waveguide mode at this m-th slice is to lowest order in the grating index modulation given by

$$r_m = -\frac{\kappa \cos(2\pi m/M)}{2\cos^2\theta} 2\pi \frac{m}{M} \tag{3}$$

where $\kappa = \Delta n_g/n_{\text{eff}}$ and n_{eff} is the effective index of the waveguide mode. The electric field of the beam reflected at the m-th slice at position x_g of the grating on axis is then

$$E_m(x_g) = a(x_m) r_m f\left[2(x_g - x_m)\cos\theta\sin\theta\right] e^{-i\beta\left[x_m + (x_m - x_g)(1-2\sin^2\theta)\right]}. \tag{4}$$

Here, $a(x)$ is the amplitude of the propagating mode field at position x and $\beta = 2\pi n_{\text{eff}}/\lambda$ is the propagation constant of the waveguide mode. The exponential term in Eq. (4) accounts for the phase of the light propagating from the start of the waveguide to position x_m and after reflection to position x_g. Finally, the total electric field of the light diffracted out of the grating is calculated as $E(x_g) = \sum_m E_m(x_g)$ in the limit of $M \to \infty$ by replacing the sum with an integral and yields

$$\begin{aligned} E\left(x_g\right) = &- a(x_g)\frac{1}{2\cos^2\theta}\frac{w}{\sin 2\theta}\frac{\kappa\pi^{3/2}}{\Lambda} \\ &\times \exp\left[-\left(\frac{w}{2\sin 2\theta}\right)^2\left(2\beta\cos^2\theta - \frac{2\pi}{\Lambda}\right)^2\right]\exp\left[-ix_g\left(\beta - \frac{2\pi}{\Lambda}\right)\right]. \end{aligned} \tag{5}$$

Here, we defined an effective width w of the grating as

$$\frac{1}{w^2} = \frac{1}{w_0^2} + \frac{1}{\sigma^2}, \tag{6}$$

to simplify the expression in Eq. (5).

The final term in Eq. (5) corresponds to the emission of a plane wave with propagation constant in the x direction of $k_x = \beta - 2\pi/\Lambda$ and therefore propagating at an angle ϕ to the negative x axis given by $k_x = -n_{\text{co}} k \cos(\phi)$ where k is the vacuum propagation constant of the light. This propagation direction of the emitted wave is therefore only dependent on the periodicity of the

grating, and not on the tilt angle. The first term in the second line of Eq. (5) is dependent on the tilt angle θ and is maximized to 1 if $2\beta\cos^2\theta - 2\pi/\Lambda = 0$. If we approximate $n_{\text{eff}} \approx n_{\text{co}}$ this condition becomes $\phi = 2\theta$, i.e., is fulfilled if the reflection of a single tilted grating plane is in the same direction as the grating diffracting direction. This is equivalent to the well known case of a blazed grating.

From Eq. (5) we obtain the reflectance of optical power per unit length [23], or in other words the fraction of optical power coupled out of the waveguide per unit length, as

$$\alpha = \frac{\sqrt{2\pi}}{w_0}\left(\frac{1}{2\cos^2\theta}\right)^2\left(\frac{\pi}{\Lambda}\right)^2\left(\frac{w}{\sin 2\theta}\right)^2\left(\frac{\Delta n_{\text{g}}}{n_{\text{eff}}}\right)^2 \exp\left[-2\left(\frac{\pi w}{\sin 2\theta}\right)^2\left(\frac{2n_{\text{eff}}\cos^2\theta}{\lambda} - \frac{1}{\Lambda}\right)^2\right]\sin\phi, \tag{7}$$

where the last term of $\sin\phi$ takes into account the angle of the emitted light.

The derivation above is given for s-polarized light and we will focus on this also in the rest of the paper. We note, however, that the reflectance for p-polarization only differs by a factor

$$\left|\frac{r_p}{r_s}\right|^2 = \cos^2 2\theta \tag{8}$$

because of the difference in Fresnel reflection coefficients r_p and r_s for p and s polarization, respectively [23]. Thus, diffracting of p-polarized light is generally weaker and vanishes completely at 90° emission ($\theta = 45°$).

3.2. Parameter dependence of reflectance

We now investigate the properties of the reflectance calculated analytically for uniform gratings by the beam tracing method in Eq. (7) and compare the results with finite-element simulations for verification. The parameters used in the following are three diffraction angles of $\phi = 60°$, 90°, and 120°, core refractive index of 1.4608, cladding index of 1.4555, grating index modulation of $\Delta n_g = 5\times10^{-3}$, index of UV-written waveguide $\Delta n = 5\times10^{-3}$, waveguide width σ =3 µm and operating wavelength λ =780 nm. The resulting effective index of the waveguide mode is $n_{\text{eff}} = 1.4640$. The value of Δn_g is chosen from the upper limit of what can be achieved with current direct UV-writing technology [18, 19, 21]. For the finite element simulations we use a grating length of 100 µm with a raised-cosine shaped apodization region of length 10 µm at both ends. We note however that our derivations and models are equally applicable to other wavelengths and other materials.

In Fig. 2(a) we show the reflectance of a 100 μm long grating for the parameters given above for three diffraction angles as a function of the refractive index modulation Δn_g of the Bragg grating, defined as the fraction of input power that is diffracted over the full grating length. In each case, the grating tilt angle is chosen as $\theta = \frac{1}{2}\cos^{-1}\left(\frac{\lambda}{n_{\text{eff}}\Lambda_g} - 1\right)$ to maximize reflection as discussed above. Then, as shown in Eq. (7), the exponential term tends to one for a short, weak grating, and the dependence becomes quadratic in index modulation. The analytical curves agree very well with the reflectance obtained from finite element simulations, given by the discrete data points in the figure. Note that the analytical result predicts the same reflectance at angles $\phi = 60°$ and $\phi = 120°$. Despite choosing the maximum index modulation that could be achieved experimentally, the coupling efficiency of such a short grating is limited to approximately 10%. Fig. 2(b) shows the reflectance for a much longer grating of 10 mm length versus Δn_g. This demonstrates that for such grating lengths a more modest index modulation of 2×10^{-3} is sufficient to couple about 90% of the light out of the waveguide.

Next, we investigate the dependence of the reflectance on the light wavelength and on the grating tilt angle in Fig. 3. Here we fix the grating index modulation at $\Delta n_g = 4\times10^{-3}$. The grating period is set to emit light at angles $\phi = 60°$, 90°, and 120° at the design wavelength of 780 nm.

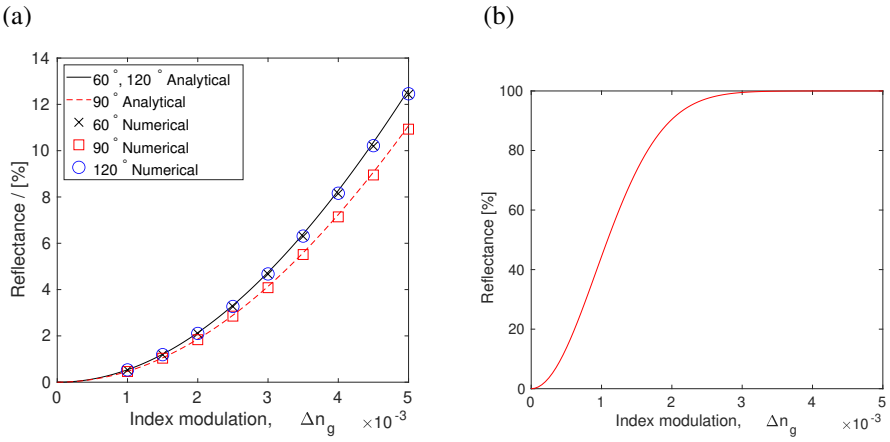

Fig. 2. (a) Reflectance of a 100 µm long grating versus grating index modulation calculated analytically by Eq. (7) (solid lines) and by FEM simulations (points) for three different diffraction angles ϕ. (b) Reflectance of a 10 mm long grating against the grating index modulation for $\phi = 90°$. Parameters are given in the text.

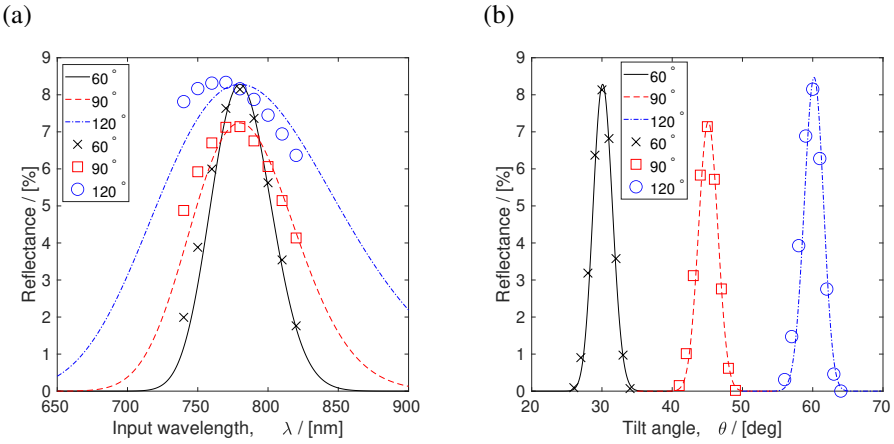

Fig. 3. Reflectance of a 100 µm long grating versus (a) input wavelength and (b) grating tilt angle at three different emission angles ϕ. Continuous curves: analytic solution, data points: FEM simulations. All parameters are given in the text.

The analytic solution, Eq. (7), is a Gaussian as a function of the propagation constant β and thus approximately Gaussian versus wavelength. The dependence on the tilt angle θ is more complex, though in lowest order close to the maximum at $2\theta \simeq \phi$ is also approximately Gaussian as seen in Fig. 3. The full widths at half maximum (FWHM) for the input wavelength dependence and tilt angle are 50.7 nm, 3.21° at 60°, 87.3 nm, 3.21° at 90°, 151.8 nm, 3.20° at 120°, respectively. We note that the FWHM versus wavelength becomes narrower for smaller angles ϕ. This is because for mostly backwards reflection, more grating planes contribute to the beam reflection and thus provide a narrower resonance, in line with standard back reflecting waveguide or fiber gratings. The same effect also leads to stronger maximum reflection for smaller ϕ. On the other hand, for larger angles ϕ and thus larger tilt angles θ the reflectance also increases because at more grazing incidence of the waveguide mode on the tilted Bragg planes the Fresnel coefficient increases. The interplay between these two effects means that a minimum of overall reflectance is found at

normal emission, $\phi = 90°$, as indicated in Fig. 3. The FWHM with respect to tilt angle only shows a very weak dependence on the emission direction.

These FWHMs suggest that UV-written gratings have a broad wavelength bandwidth but that the tilt angle needs to be fabricated with care. However, as previously mentioned in Sec. 3.1, the grating period relative to the wavelength affects the direction of the out-coupled beam (final term in Eq. (5)); therefore, while the coupling efficiency may not change significantly with small wavelength changes, the propagation direction of the out-coupled beam in free space above the chip will change.

Comparison of the analytic results in Fig. 3 with the results of FEM simulations exhibits some minor discrepancies due to the simplifying approximations in the analytic derivation, e.g. that it only considers the first order perturbation of the grating index modulation and ignores the effects of refraction of the diffracted beam within the position-dependent refractive index of the waveguide. These neglected higher order effects become more pronounced at grazing incidence of the waveguide mode field on the grating planes, i.e., at angles of $\theta \gtrsim 120°$ as can be seen in Fig. 3(a). However, in general the results agree well and give confidence in the analytical solution as a means to design more complex grating structures and thus waveguide devices for out-of-plane beam delivery on a chip, as discussed in the following sections.

4. Beam shaping

4.1. Grating design

We can now use the theory described above to design gratings that generate a specific out-coupled beam and direct it at a target location. For example, for applications in quantum technology we may wish to generate a beam that is focused onto a single trapped ion or a cloud of trapped neutral atoms at a certain distance above the chip.

To keep the grating design realistic for fabrication, we assume that the tilt angle θ is fixed, which as shown in Fig. 3(b) limits the achievable angles to a cone around $\phi = 2\theta$. The grating index distribution is thus of the form

$$n_g\,(x, y) = n_{co} + \left[\Delta n + \Delta n_g(x)\,\sin\!\left(\left(\frac{2\pi}{\Lambda} + \frac{2\pi n_{\text{eff}}}{\lambda}\cos\phi\right)(x - y\tan\theta) + \Phi(x)\right)\right] e^{-\left(\frac{y}{\sigma}\right)^2}. \quad (9)$$

For a grating to generate the desired out-coupled beam, the grating index modulation $\Delta n_g(x)$ and an added position-dependent phase $\Phi(x)$ that induces the local phase, as shown in Eq. (9), are needed which will determine the shape and the directionality of the beam, respectively.

We first have to calculate the desired electric field at the position of the grating. If we know the field at the target position, see Fig. 1, we obtain the field at the center of the grating (i.e. at $y = 0$) by propagating the target field via an angular spectrum method, i.e., we Fourier transform the field at y_{target} and subsequently propagate the field analytically from y_{target} to $y = 0$, taking into account refraction of the field at dielectric interfaces. Let us write this target electric field at the grating as a real-valued amplitude $E_0(x)$ and a complex phase $\Phi_{\text{el}}(x)$,

$$E(x) = E_0(x)e^{-i\Phi_{\text{el}}(x)}. \quad (10)$$

Here we assume s-polarization only and thus write a scalar electric field. By comparing these expressions with Eqs. (1), (5) we see that the required phase of the grating is simply equal to the target electric field phase, $\Phi = \Phi_{\text{el}}$.

The calculation of the grating index modulation $\Delta n_g(x)$ is more complicated as we need to take into account depletion of the pump field propagating in the waveguide. We first introduce the intensity of the out-coupled beam

$$I(x) = C|E_0(x)|^2 \quad (11)$$

where C is a normalization constant. Integrated along the length of the grating, this gives the total power coupled into the target beam

$$P_{\text{out}} = C \int_0^L |E_0(x')|^2 \, dx' = \eta P_0 \tag{12}$$

where L is the device length, P_0 is the pump power coupled into the waveguide at $x = 0$ and η is the fraction of waveguide power coupled into the target beam. Equating the pump depletion to the out-coupled beam intensity,

$$-dP(x)/dx = P(x)\alpha(x) = I(x) \tag{13}$$

and using power conservation

$$P(x) = P_0 - \int_0^x I(x')dx' \tag{14}$$

we obtain from Eq. (7) the required grating index modulation

$$\Delta n_{\text{g}}^2(x) = \frac{w_0}{\sqrt{2\pi}} \left(\frac{\lambda \sin(2\theta)}{w\pi} \right)^2 \frac{1}{\sin\phi} \frac{|E_0(x)|^2}{P_0 - C\int_{-\infty}^{x} |E_0(x')|^2 \, dx'}. \tag{15}$$

Here we fixed the grating period Λ to give optimum coupling efficiency for tilt angle θ. When $\eta = 1$, all the pump light is outputted from the grating but this may lead to unfeasible, large grating index modulations. Reducing η and thus the power of the out-coupled beam, while maintaining its spatial profile proportional to $E(x)$, allows us to control the grating index modulation within realistic values.

4.2. Numerical examples of beam shaping

In this section, two types of grating are designed to demonstrate our beam shaping method with direct UV-written gratings: a super-Gaussian (flat top) beam and a multi-Gaussian beam. The refractive indices chosen are the same as given in Sec. 3.2, except for Δn_g which has been exaggerated up to 1.83×10^{-2} for enhanced grating coupling to allow for comparison with small-scale FEM simulations. The height of the core layer is 5 µm, and the overcladding thickness is 15 µm.

In the first example we want to generate a super-Gaussian beam of order 10 with a spot size of $W = 20\,\mu\text{m}$ located at position $x_{\text{target}} = -30\,\mu\text{m}$, $y_{\text{target}} = 100\,\mu\text{m}$ defined as

$$E(x, y_{\text{target}}) = e^{-ik_0 \cos\phi} e^{-\left(\frac{x - x_{\text{target}}}{W}\right)^{20}}, \tag{16}$$

where the angle ϕ is chosen such that the grating is centered around $x = 0$. The numerical simulations generating this beam using the beam shaping method described in Sec. 4.1 are shown in Fig. 4.

As explained in Section 4.1, the field at $y = 0$ is calculated from the target field (16) by an angular spectrum method, thus taking into account diffraction and refraction effects between grating and target position. Next, the required grating index profile is calculated, Eq. (15) and is implemented in a FEM model. The bottom of Fig. 4(a) shows the resulting light propagation through waveguide and grating. The out-coupled field is then extracted from the FEM simulation and is propagated through the device overcladding and free space by the angular spectrum method, shown at the top of Fig. 4(a). The red dashed line shows the target plane and the black-solid line shows the boundary between the glass layer and free space. Figure 4(b) compares the target field shape (blue dashed line) with the field generated by the numerical simulations in (a) (red solid

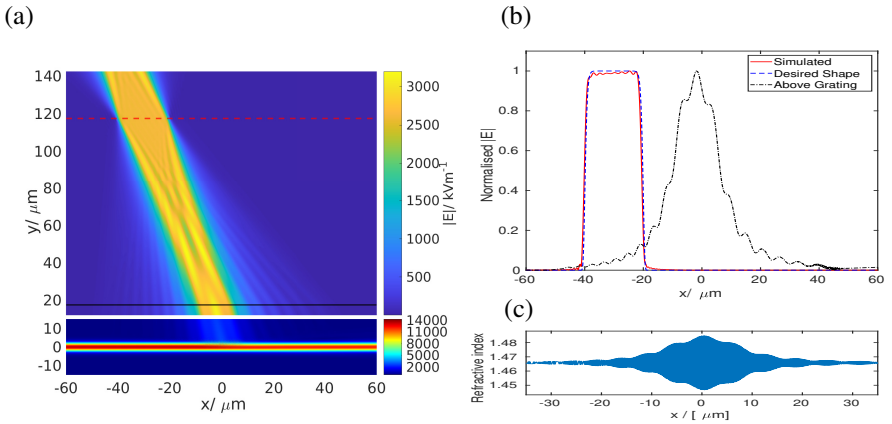

Fig. 4. Generation of a super-Gaussian of order 10. (a) Bottom: light propagation in the waveguide and grating simulated by FEM. Top: propagation of the out-coupled light into free space by angular spectrum method. (b) Out-coupled field at the grating position (green dash-dotted) and at the target position (red solid) and the original target field (blue dashed). (c) Corresponding grating refractive index profile.

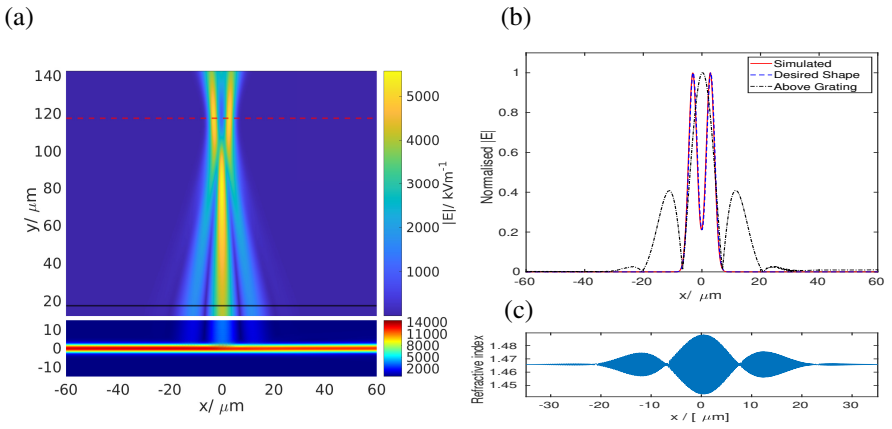

Fig. 5. Generation of a multi-Gaussian beam with two different spots in the target plane. (a) Light propagation simulation using FEM (bottom) and subsequent angular spectrum method (top). (b) Target and simulated light fields on the grating and at the target position. (c) Corresponding grating refractive index profile.

line). We also show the shape of the out-coupled field just above the grating. The corresponding grating refractive index profile is given in Fig. 4(c). The example shows good agreement between the target and the simulated field, demonstrating our grating design method.

In our second example we demonstrate a grating design where a single grating generates two Gaussian beams focused at separate positions, e.g., to illuminate two single trapped ions in a chip-based quantum information processor with a minimum of light diffracted into other directions. Here our target is to achieve two beams with 2 µm spot situated 100 µm above the surface and separated by 6 µm; all other parameters are as above.

The method is the same as in the super-Gaussian beam example above and the results are shown in Fig. 5. We can clearly see the emission of the target light field from the grating and the formation and focusing of the two Gaussian beams in Fig. 5(a). Comparison between the target and the simulated fields, Fig. 5(b), again show good agreement.

4.3. Coupling efficiency

Having introduced and numerically verified the principles of our beam-shaping method above, we will now use our analytic formula to discuss beam shaping for experimentally realistic parameters, i.e., with lower grating index modulations and longer grating lengths of mm instead of tens of µm in the examples above.

We start with designing a grating to achieve a Gaussian output beam at an angle of $\phi = 60°$, i.e., backward diffracted at a tilt of 30° from the normal to the surface of the grating, similar to the beam in Fig. 4. The target location is 5 mm above the chip with 10 µm beam waist. The grating index modulation is restricted to the highest realistic value at 5×10^{-3}.

Using the formulas from Sec. 4.1 we calculate the grating index modulation and position-dependent grating period needed to produce such a Gaussian beam, shown in Fig. 6(a). Here we use the position-dependent grating period

$$\Lambda(x) = 2\pi \left| \frac{2\pi n_{\text{eff}}}{\lambda} + \frac{d\Phi}{dx} \right|^{-1} \tag{17}$$

as an alternative and more intuitive grating parameter than the position-dependent phase Φ of Eq. (9). The required shape of the grating strength is again approximately given by a Gaussian. The local grating period is decreasing along the grating to produce the correct curved phase front of the out-coupled electric field to create the focusing Gaussian beam. In other words, the light coupled out of the grating at the beginning at the grating needs to travel in a more forward direction (longer local period) than light coupled out at the end of the grating (shorter period) to focus light into a point above the surface.

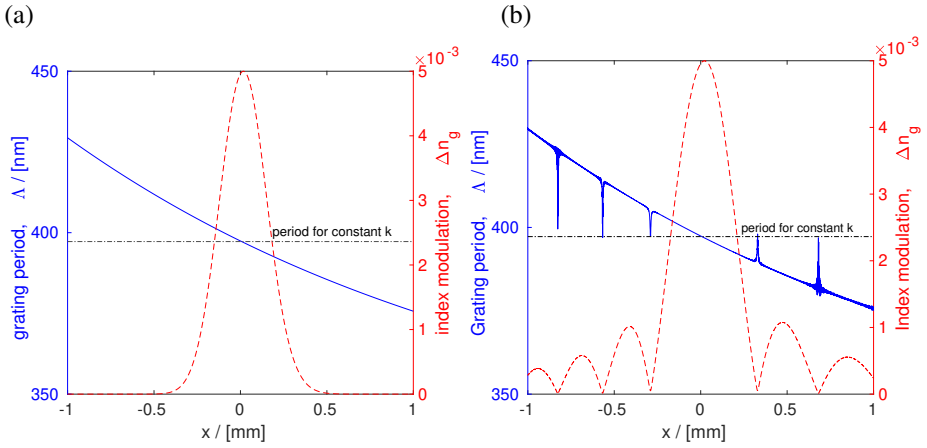

Fig. 6. Grating designs for the generation of (a) a Gaussian beam, (b) a super-Gaussian beam with 10 µm waist at 5 mm above the chip propagating at an angle of 60°. Red dashed line (right axis): required grating index modulation with maximum set at 5×10^{-3}; Blue solid line (left axis): local grating period. The black dash dotted line represents the constant grating period needed for emission at 60°.

In calculating the grating properties above we have chosen the normalization constant C in Eq. (11) such that the maximum grating index modulation does not exceed 5×10^{-3}. Thus, by substituting the grating period and grating index modulation calculated above into the analytic solution, Eq. (12), the total coupling efficiency of the grating can be found. For the example of Fig. 6(a) this is 25.1 % of the input power. This is limited by the achievable grating strength and the length of the grating. Larger efficiencies would require stronger index modulation, which is not currently achievable by direct UV writing in silica but may be possible in more photosensitive

materials or by other grating technologies such as etching, or longer gratings, which require to move to beam focus further away from the chip surface.

In Fig. 6(b) we show the required grating parameters to form a super-Gaussian beam of order 10, with other parameters the same as for the Gaussian beam in (a). In this case the required grating strength approaches a sinc function (which is the Fourier transform of a flat top beam) and thus is significantly wider than for the Gaussian beam. The local grating period $\Lambda(x)$ follows a similar decreasing trend as for the Gaussian case but shows peaks at positions where the grating strength vanishes and hence the local phase and grating period are not well defined. In practice, these positions correspond to π phase shifts when the sinc function changes sign.

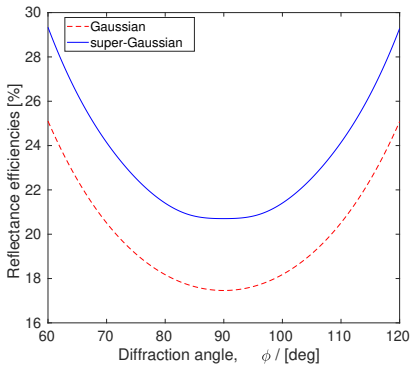

Fig. 7. Total diffracting efficiency η of gratings optimized for generating Gaussian and super-Gaussian beams with waist 10 µm and at 5 mm above the chip surface against the out-coupling angle ϕ. Other parameters as in Fig. 6.

Finally, we show the total coupling efficiency η for Gaussian and super-Gaussian beam generation versus output angle ϕ in Fig. 7, where at each angle ϕ the grating tilt angle θ is optimized to achieve maximum coupling. More light is coupled from the waveguide into a super-Gaussian beam than a fundamental Gaussian beam since the super-Gaussian has a larger beam divergence and is therefore generated by a longer grating, as already seen in Fig. 6.

For both beam shapes and as already discussed in Sec. 3.2, the coupling efficiency is minimum at $\phi = 90^\circ$ but increases towards smaller angles because of a larger number of contributing grating planes and towards larger angles because of larger Fresnel reflections off the tilted grating planes at grazing incidence. Fig. 7 thus suggests that angled out-coupling grating designs might be more useful than their non-angled counterparts for the integration into quantum devices because of the higher efficiencies.

5. Conclusion

We have derived an analytic expression that describes the coupling efficiency of tilted UV-written Bragg gratings for the generation of out-of-plane light beams above the chip surface. The analytic result has been tested against finite element simulations and a method to generate any specific target beam shape has been presented and discussed.

Applications of our work will be found in the area of quantum technology. For example, such tilted Bragg gratings could be used to illuminate and coherently address trapped atoms and ions for quantum information processing or quantum sensing using integrated photonics, significantly improving scalability of such devices compared to using free space optics.

For realistic experimental parameters the specific approach modelled here, direct UV writing, limits the maximum Bragg grating index contrast and thus we find overall coupling efficiencies of light from the waveguide into the target shaped beam of the order of 10% or less for small

beams focused close to the chip surface, whereas millimeter length scale devices can work with close to 100% efficiency.

Funding. UK Engineering and Physical Sciences Research Council EPSRC (UK Quantum Technology Programme, EP/M013243/1, EP/T001062/1); Innovate UK ("QT Assemble", reference 50414).

Disclosures. The authors declare no conflicts of interest.

Data Availability. Data underlying the results presented in this paper are available in Ref. [24].

References

1. K. Bong, M. Holynski, J. Vovrosh, P. Bouyer, G. Condon, E. Rasel, C. Schubert, W. P. Schleich, and A. Roura, "Taking atom interferometric quantum sensors from the laboratory to real-world applications," Nat. Rev. Phys. **1**, 731–739 (2019).
2. A. Gialopsou, C. Abel, T. James, T. Coussens, M. Bason, R. Puddy, F. Di Lorenzo, K. Rolfs, J. Voigt, T. Sander, M. Cercignani, and P. Krüger, "Improved spatio-temporal measurements of visually evoked fields using optically-pumped magnetometers," Sci. Rep. **11**, 22412 (2021).
3. A. B. Price, J. G. Rarity, and C. Erven, "A quantum key distribution protocol for rapid denial of service detection," EPJ Quantum Technol. **7**, 8 (2020).
4. J. M. Pino, J. M. Dreiling, C. Figgatt, J. P. Gaebler, S. A. Moses, M. S. Allman, C. H. Baldwin, M. Foss-Feig, D. Hayes, K. Mayer, C. Ryan-Anderson, and B. Neyenhuis, "Demonstration of the trapped-ion quantum CCD computer architecture," Nature **592**, 209–213 (2021).
5. J. E. Bourassa, R. N. Alexander, M. Vasmer, A. Patil, I. Tzitrin, T. Matsuura, D. Su, B. Q. Baragiola, S. Guha, G. Dauphinais, K. K. Sabapathy, N. C. Menicucci, and I. Dhand, "Blueprint for a Scalable Photonic Fault-Tolerant Quantum Computer," Quantum **5**, 392 (2021).
6. A. P. M. Place, L. V. H. Rodgers, P. Mundada, B. M. Smitham, M. Fitzpatrick, Z. Leng, A. Premkumar, J. Bryon, A. Vrajitoarea, S. Sussman, G. Cheng, T. Madhavan, H. K. Babla, X. H. Le, Y. Gang, B. Jack, A. Gyenis, N. Yao, R. J. Cava, N. P. de Leon, and A. A. Houck, "New material platform for superconducting transmon qubits with coherence times exceeding 0.3 milliseconds," Nat. Commun. **12**, 1779 (2021).
7. R. Niffenegger, C. Sorace-Agaskar, D. Kharas, S. Bramhavar, C. Bruzewicz, W. Loh, R. Maxson, R. McConnell, D. Reens, G. West, J. Sage, and J. Chiaverini, "Integrated multi-wavelength control of an ion qubit," Nature **586**, 538–542 (2020).
8. W. R. McGehee, W. Zhu, D. S. Barker, D. Westly, A. Yulaev, N. Klimov, A. Agrawal, S. Eckel, V. Aksyuk, and J. J. McClelland, "Magneto-optical trapping using planar optics," New J. Phys. **23**, 013021 (2021).
9. M. Gehl, W. Kindel, N. Karl, A. Orozco, K. Musick, D. Trotter, C. Dallo, A. Starbuck, A. Leenheer, C. DeRose, G. Biedermann, Y.-Y. Jau, and J. Lee, "Characterization of suspended membrane waveguides towards a photonic atom trap integrated platform," Opt. Express **29**(9), 13129–13140 (2021).
10. J. P. McGilligan, K. R. Moore, A. Dellis, G. D. Martinez, E. de Clercq, P. F. Griffin, A. S. Arnold, E. Riis, R. Boudot, and J. Kitching, "Laser cooling in a chip-scale platform," Appl. Phys. Lett. **117**, 054001 (2020).
11. C. Roos, *Quantum Information Processing with Trapped Ions* (Springer, 2014), vol. 256, pp. 253–291.
12. C. Bruzewicz, J. Chiaverini, R. McConnell, and J. Sage, "Trapped-ion quantum computing: Progress and challenges," Appl. Phys. Lett. **6**, 021314 (2019).
13. S. Ura, A. Sugimoto, T. Suhara, and H. Nishihara, "Integration of grating couplers in two-story waveguides for rotary displacement sensing," Appl. Opt. **37**(27), 6345–6349 (1998).
14. Y. Tang, Z. Wang, L. Wosinski, U. Westergren, and S. He, "Highly efficient nonuniform grating coupler for silicon-on-insulator nanophotonic circuits," Opt. Lett. **35**(8), 1290–1292 (2010).
15. S. Kerman, D. Vercruysse, T. Claes, A. Stassen, M. Mahmud ul Hasan, P. Neutens, V. Mukund, N. Verellen, X. Rottenberg, L. Lagae, and P. Van Dorpe, "Integrated Nanophotonic Excitation and Detection of Fluorescent Microparticles," ACS Photonics **4**, 1937–1944 (2017).
16. S. Kim, D. A. Westly, B. J. Roxworthy, Q. Li, A. Yulaev, K. Srinivasan, and V. A. Aksyuk, "Photonic waveguide to free-space Gaussian beam extreme mode converter," Light Sci. Appl. **7**, 72 (2018).
17. M. Svalgaard, C. Poulsen, A. Bjarklev, and O. Poulsen, "Direct UV writing of buried singlemode channel waveguides in Ge-doped silica films," Electron. Lett. **30**, 1401–1403 (1994).
18. C. Sima, J. C. Gates, H. L. Rogers, P. Mennea, C. Holmes, M. N. Zervas, and P. G. R. Smith, "Ultra-wide detuning planar Bragg grating fabrication technique based on direct UV grating writing with electro-optic phase modulation," Opt. Express **21**(13), 15747–15754 (2013).
19. J. W. Field, S. A. Berry, R. H. Bannerman, D. H. Smith, C. B. Gawith, P. G. Smith, and J. C. Gates, "Highly-chirped Bragg gratings for integrated silica spectrometers," Opt. Express **28**(14), 21247–21259 (2020).
20. S. Srikanth, S. Dudala, S. Raut, S. K. Dubey, I. Ishii, A. Javed, and S. Goel, "Optimization and characterization of direct UV laser writing system for microscale applications," J. Micromech. Microeng. **30**, 095003 (2020).
21. Q. Salman Ahmed, P. Gow, C. Holmes, P. Mennea, J. Field, R. Bannerman, D. Smith, C. Gawith, P. Smith, and J. Gates, "Direct UV written waveguides and Bragg gratings in doped planar silica using a 213 nm laser," Electron. Lett. **57**(8), 331–333 (2021).

22. M. T. Posner, N. Podoliak, D. H. Smith, P. L. Mennea, P. Horak, C. B. E. Gawith, P. G. R. Smith, and J. C. Gates, "Integrated polarizer based on 45° tilted gratings," Opt. Express **27**(8), 11174 (2019).
23. T. Yoshino, "Theoretical analysis of a tilted fiber grating polarizer by the beam tracing approach," J. Opt. Soc. Am. B **29**(9), 2478 (2012).
24. D. Ko, Q. Salman Ahmed, J. W. Field, J. C. Gates, and P. Horak, "Dataset for Out-of-plane beam shaping with UV-written tilted Bragg gratings for beam delivery on quantum chips," University of Southampton (2022), http://doi.org/10.5258/SOTON/D2305.